Astronomy
&
Astrophysics

The changing look of PKS 2149-306

V. Bianchin[1], L. Foschini[1], G. Ghisellini[2], G. Tagliaferri[2], F. Tavecchio[2], A. Treves[3], G. Di Cocco[1], M. Gliozzi[4], E. Pian[5], R. M. Sambruna[6], and A. Wolter[2]

[1] INAF/IASF-Bologna, via Gobetti 101, 40129 Bologna, Italy
  e-mail: bianchin@iasfbo.inaf.it
[2] INAF - Osservatorio Astronomico di Brera, via E. Bianchi 46, 23807 Merate, Italy
[3] Dipartimento di Scienze, Università dell'Insubria, Como, Italy
[4] George Mason University, 4400 University Drive, Fairfax, Va 22030, USA
[5] INAF - Osservatorio Astronomico di Trieste, via G. B. Tiepolo 11, 34131 Trieste, Italy
[6] NASA Goddard Space Flight Center, Code 661, Greenbelt, MD 20771, USA

ABSTRACT

Aims. We study the blazar nature of the high-redshift Flat-Spectrum Radio Quasar PKS 2149-306 ($z = 2.345$) by investigating its long-term behavior.
Methods. We analyzed all publicly available optical-to-X-ray observations performed by *XMM-Newton*, *Swift*, and *INTEGRAL*.
Results. PKS 2149-306 is one of four blazars at $z > 2$ that have been observed in the hard-X-ray regime with both the BAT and ISGRI instruments. Observations acquired almost 1 year apart in the $60-300$ keV energy band in the object rest frame, exhibit no noticeable change in spectral slope associated with a flux variation of more than a factor of two. *Swift* data appear to show a roll-off below ~1 keV, which becomes increasingly evident during a ~3-day time-frame, that can be explained as the natural spectral break caused by the Inverse Compton onset. The broad-band spectra allow us to identify two different states. The SED modeling suggests that they can be interpreted by only a change in the bulk Lorentz factor of the jet.

Key words. quasars: individual: PKS 2149-306 – quasars: general – X-rays: galaxies

1. Introduction

PKS 2149-306 is a Flat Spectrum Radio Quasar (FSRQ) located at $z = 2.345$ (Wilkes 1986). In the radio maps, it exhibits a compact but non-point-like structure (e.g., Ojha et al. 2005) of ≈1 Jy flux density over a wide radio frequency range (0.8–8.4 GHz)[1]. The few observations of the optical counterpart show no significant changes in all filters with $m_V \sim 18$ (e.g., Francis et al. 2000). The object hosts a bright X-ray source extensively observed in the past by *ROSAT* and *ASCA* (Siebert et al. 1996; Cappi et al. 1997), *BeppoSAX* (Elvis et al. 2000), *Chandra* (Fang et al. 2001), *XMM-Newton* (Ferrero & Brinkmann 2003), and more recently by *Swift* (Sambruna et al. 2007). In the X-ray domain, the source exhibits a hard spectrum with variable photon index and flux. From early *ASCA* observations, the presence of an emission line at ≈17 keV in the blazar frame was interpreted as a highly-blueshifted Fe Kα line produced by an outflow at speed $v \sim 0.7c$ (Yaqoob et al. 1999); however, *Chandra* high-resolution spectroscopy did not confirm this finding (Fang et al. 2001). Page et al. (2004) found no evidence for a disk/torus Fe Kα emission line.

As for other high-z FSRQs, a controversial low-energy photon deficit has been claimed by some authors but not confirmed by others (Siebert et al. 1996; Cappi et al. 1997; Yaqoob et al. 1999; Sambruna et al. 2007; Elvis et al. 2000; Ferrero & Brinkmann 2003; Page et al. 2005). This putative deficit was usually ascribed to an absorbing cloud in the quasar reference frame and modeled by additional intrinsic absorption in addition

to the Galactic one. However, considering the blazar nature of PKS 2149-306, it is difficult to explain how an absorbing cloud can survive in front of a jet. On the other hand, interpreting this flux deficit as a natural break in the Spectral Energy Distribution (SED) due to the low-energy tail of the electron population leads to a coherent explanation of the observed spectral changes in PKS 2149-306 (cf. the case of RBS 315, Tavecchio et al. 2007).

PKS 2149-306 is one of the few FSRQs observed in the hard-X-ray regime after the *BeppoSAX* era (Elvis et al. 2000). A recent *Swift* observation (Sambruna et al. 2007) confirmed that the source displays a Compton-dominated spectrum, typical of FSRQs, with a Compton peak probably located at approximately hundreds of keV (observer frame).

In this work, we present a serendipitous detection of PKS 2149-306 in *INTEGRAL* archival data. To date, the source catalog of the *INTEGRAL*/ISGRI detector (Lebrun et al. 2003) includes 18 blazars, among which 6 are located at $z > 2$ (e.g., Bird et al. 2008). The AGN catalog of the *Swift*/BAT instrument (Barthelmy et al. 2005) contains comparable numbers, with 6 high-redshift objects (Baumgartner et al. 2008). Including PKS 2149-306, there are only four objects detected by both ISGRI and BAT. We performed a spectral analysis of *INTEGRAL* data reanalyzed all publicly available data for the source from the *XMM-Newton* and *Swift* archives. Here, we discuss the broadband spectral variation of the source over several years.

2. Data analysis

Table 1 lists all observations of PKS 2149-306 analyzed in this paper, including starting dates and exposure times. For all

---

[1] Data from NASA/IPAC Extragalactic Database (NED) http://nedwww.ipac.caltech.edu/index.html.

Table 1. Observation Log.

Instrument	ObsID	Start date [YYYY-MM-DD]	Exposure [ks]
INTEGRAL/ISGRI	Rev. 254, 258-260	2004-11-11	366
XMM/EPIC	0103060401	2001-05-01	20
Swift/XRT (OBS. 1)	00035242001	2005-12-10	3.1
Swift/XRT (OBS. 2)	00035242002	2005-12-13	2.3
Swift/BAT	9-month Survey	mid Dec. 2005	2800

For each instrument, the table indicates the observation ID or the revolution number, the starting date of the observation, and the effective exposure for PKS 2149-306. BAT data refer to the 9-month survey, starting in mid-December 2005. BAT exposure time is computed by integrating over all pointings with the source PKS 2149-306 within the FOV of the BAT instrument.

observatories, data were processed using the latest versions of the specific software and calibration files. The output spectra of *XMM-Newton*/EPIC and *Swift*/XRT were rebinned to contain at least 30 counts per bin. Spectral analysis was carried out by means of xspec v.12.4.0. In all X-ray model fits, we included Galactic extinction and fixed the column density to be $N_H = 1.63 \times 10^{20}$ cm^{-2} (Kalberla et al. 2005). Our fit results are given in Table 2.

2.1. INTEGRAL

We achieved a serendipitous detection of PKS 2149-306 using the *INTEGRAL* public archive data; the source was in the IBIS (Ubertini et al. 2003) field of view during November 2004 (Revolutions 254, 258 − 260), while pointing to NGC 7172. Data were analyzed with the Off-line Scientific analysis Software OSA 7.0 (Courvoisier et al. 2003). The imaging analysis of IBIS/ISGRI data (Goldwurm et al. 2003) provided a source detection of signal-to-noise ratio $S/N = 4$ in the 20−100 keV energy band with exposure of 366 ks. The faint detections in single pointings did not allow us to inspect light curve variations. The total spectrum was extracted using a rebinned response matrix with 5 energy bins in the energy range 20−140 keV. The ISGRI spectrum can be modeled by a single power-law with photon index $\Gamma = 1.5^{+0.9}_{-0.8}$ and flux $(2.1 \pm 0.2) \times 10^{-11}$ erg cm^{-2} s^{-1} in the 20−100 keV energy band (Table 2).

The source is below the capabilities of both JEM-X and PICsIT instruments, with upper limits of 10^{-11} erg cm^{-2} s^{-1} in 8−14 keV and 3.5×10^{-10} erg cm^{-2} s^{-1} in 252−336 keV respectively.

SPI data were not considered since the source NGC 7172, the primary target of the observations, falls on the border of the instrument Point-Spread Function (PSF) (2.5 degrees) centered on PKS 2149-306.

OMC data were not included in the analysis because a contaminating source is located within the instrumental 25 arcsec PSF FWHM of PKS 2149-306 (see the *Swift*/UVOT data analysis below).

2.2. XMM-Newton

XMM-Newton observed PKS 2149-306 on May 1, 2001, starting at 10:53 UT (ObsID 0103060401). We reanalyzed these data, already presented by Ferrero & Brinkmann (2003). Data from EPIC-PN (Strüder et al. 2001), EPIC-MOS (Turner et al. 2001) and OM (Mason et al. 2001) were processed, screened, and analyzed using the same procedure described in Foschini et al. (2006), but with the SAS v 7.1.0 software and

calibration file release of July 16, 2007. No periods of high-background were detected, and the net exposures with the individual detectors were 20.3 ks with PN and 24 ks with MOS1 and MOS2.

The EPIC-PN light curve (not shown here) displays no significant flux changes (χ^2 probability of constancy 0.43) with an upper limit to the fractional variability <3% (3σ).

Our spectral analysis confirms the results of Ferrero & Brinkmann (2003) that the best-fit model was a single power-law function with parameters reported in Table 2. The normalization constants between the MOS instruments and PN are consistent with unity ($C_{MOS1-PN} = 1.00 \pm 0.02$, $C_{MOS2-PN} = 1.03 \pm 0.02$). In panel *a* of Fig. 1, the residuals of the power-law model are plotted in units of σ and with error bars of size 1σ; for a clearer visualization, only PN data are shown. We applied more complex models: a power-law function with Galactic extinction and an absorption excess in the source frame (wabs*zwabs*zpo) and an absorbed broken power-law function (wabs*bknpo). Both provided comparable values of χ^2_r, but the parameters were not well-constrained or they converged to unphysical quantities.

We also checked for the presence of neutral iron line emission in the quasar frame but we found no indication of such a feature (confirming Page et al. 2004).

The OM observed the blazar for ~1000 s with *UVW2* filter (centered at 212 nm): no detection was found, with a magnitude lower limit of 19 (3σ), corresponding to a flux ≤3.4 × 10^{-13} erg cm^{-2} s^{-1}.

2.3. Swift

Swift observed PKS 2149-306 twice in 2005 (Sambruna et al. 2007): ObsID 00035242001 started on December 10, 2005 00:47 UT, and ObsID 00035242002 started on December 13, 2005 20:13 UT with exposure times of 3.1 ks and 2.3 ks, respectively. For the reduction and analysis of the data from the three instruments onboard the *Swift* satellite, we used the HEASoft v. 6.4 package, together with the CALDB updated on February 13, 2008.

The data from the BAT instrument (Barthelmy et al. 2005), optimized for the 15−195 keV energy band, were binned, cleaned of hot pixels, and deconvolved. The intensity maps from the individual pointings were integrated by using the corresponding variance maps as a weighting factor, and the resulting exposure simultaneous to the XRT and UVOT observations was 5.4 ks. No source was detected; the corresponding 3σ upper limits were 2.7×10^{-10} erg cm^{-2} s^{-1} and 4.3×10^{-10} erg cm^{-2} s^{-1} in the 20−40 keV and 40−100 keV energy band, respectively. However, the blazar was detected in the 9-month data survey (Tueller et al. 2008), and the source spectrum is publicly available online (Baumgartner et al. 2008). The fitting of a power-law model is optimal for a photon index of $\Gamma = 1.5 \pm 0.4$ and a flux of 4.8×10^{-11} erg cm^{-2} s^{-1} in the 20−100 keV energy band.

The X-Ray Telescope (XRT, Burrows et al. 2005), operating in the 0.2−10 keV energy band, was set to work in photon counting mode during the two pointings on PKS 2149-306. Data were processed and screened by using the xrtpipeline task with the single to quadruple pixels events selected (grades 0−12).

The spectral analysis of the XRT data was presented in Sambruna et al. (2007) as a joint fit of the two observations. Here, we consider the two data sets separately and we fit each with three models, all including Galactic extinction: a power-law (wabs*zpo), a power-law with an extra-absorption component in the source rest frame (wabs*zwabs*zpo) and a broken power-law (wabs*bknpo).

Table 2. Fit results.

Instrument	Model	Γ or Γ_1	Additional parameters		$F_{2-10\ \mathrm{keV}}$	χ_r^2/d.o.f.
		X-rays (0.2−10 keV)				
XMM/EPIC	wabs*zpo	1.42 ± 0.01			0.56 ± 0.01	1.08/977
Swift/XRT (OBS. 1)	wabs*zpo	1.44 ± 0.07			1.2 ± 0.1	1.24/29
Swift/XRT (OBS. 2)	wabs*zpo	1.38 ± 0.09			$1.04^{+0.06}_{-0.09}$	1.63/15
	wabs*zwabs*zpo	$1.55^{+0.17}_{-0.16}$	$N_z = 1.0^{+1.1}_{-0.8}\ 10^{22}\ \mathrm{cm}^{-2}$		$0.97^{+0.5}_{-0.08}$	1.42/14
	wabs*bknpo	$0.98^{+0.29}_{-0.41}$	$E_{\mathrm{break}} = 1.9^{+1.5}_{-0.6}\ \mathrm{keV}$	$\Gamma_2 = 1.86^{+1.19}_{-0.31}$	0.8 ± 0.1	0.98/13

Instrument	Model	Γ			$F_{20-100\ \mathrm{keV}}$	χ_r^2/d.o.f.
		Hard X-rays (20−100 keV)				
INTEGRAL/ISGRI	zpo	$1.5^{+0.9}_{-0.8}$			2.1 ± 0.2	0.51/3
Swift/BAT	zpo	1.5 ± 0.4			4.8 ± 0.5	0.48/2

Instrument	Model	Γ or Γ_1	Additional parameters		$F_{2-100\ \mathrm{keV}}$	χ_r^2/d.o.f.
		Joint fit (0.2−100 keV)				
EPIC+ISGRI	wabs*zpo	1.42 ± 0.01			$3.13^{+0.05}_{-0.04}$	1.08/980
XRT (OBS. 1) + BAT	wabs*zpo	1.44 ± 0.07			$6.4^{+0.9}_{-0.8}$	1.2/32
XRT (OBS. 2) + BAT	wabs*bknpo	$0.9^{+0.3}_{-0.4}$	$E_{\mathrm{break}} = 1.6^{+0.9}_{-0.4}\ \mathrm{keV}$	$\Gamma_2 = 1.7^{+0.3}_{-0.2}$	3 ± 1	0.92/16

Models and parameters for single instruments and joint fit. Applied models are: a power-law in the source rest frame (zpo), a power-law with an absorption component in the object rest frame (zwabs*zpo) and a broken power-law (bknpo). All models include Galactic absorption (wabs) with column density $N_{\mathrm{H}} = 1.63 \times 10^{20}\ \mathrm{cm}^{-2}$ (Kalberla et al. 2005). Flux is given in units of $10^{-11}\ \mathrm{erg\ cm}^{-2}\ \mathrm{s}^{-1}$.

The spectrum of the first observation (2005-12-10) is well described by a single power-law with Galactic absorption (Table 2). Residuals are shown in panel *b* of Fig. 1 (in units of 1σ). Although the broken power-law and the power-law with extra absorption models yield $\chi_r^2 = 1.2$ (for 27 and 28 d.o.f., respectively), the spectral parameters are not well constrained or they converge to unphysical values. For the second observation (2005-12-13), we found that the broken power-law function provided the best-fit model, although both the power-law model and the power-law function with an extra-absorption component described the observational data accurately. In Table 2 we present the best-fit parameters for the three applied models. The residual plot of the power-law model (Fig. 1, panel *c*) shows a hint of curvature, which is not present when the broken power-law model is assumed (Fig. 1, panel *d*). The curved model is also supported by the F-test analysis, showing that the flatter power-law function below ~1.7 keV is required with a probability of 98.6%. The quality of data acquired to date does not allow us to distinguish firmly between the intrinsically curvature (broken power-law) and the extra-absorption model.

UVOT (Roming et al. 2005) data analysis was performed by the uvotmaghist task using a source region of 5″ radius for the optical and 10″ for the UV filters. Since a contaminating source is located close to PKS 2149-306, the background was evaluated from a nearby region of 60″ radius. The observed magnitudes were computed as the mean values of recorded data, since they do not exhibit significant variations: $V_{543\ \mathrm{nm}} = 17.4 \pm 0.2$, $B_{434\ \mathrm{nm}} = 17.7 \pm 0.1$, $U_{344\ \mathrm{nm}} = 17.1 \pm 0.1$, $UVW1_{291\ \mathrm{nm}} = 17.9 \pm 0.2$, $UVM2_{231\ \mathrm{nm}} \geq 19.1$, and $UVW2_{212\ \mathrm{nm}} \geq 19.4$. The optical magnitudes are in accordance with values observed by Francis et al. (2000). With respect to the previous analysis of Sambruna et al. (2007), we obtain comparable magnitudes for all filters but $UVM2$ and $UVW2$, for which we found an upper limit. The discrepancy is probably due to the use of updated calibration files.

2.4. Joint fits

We attempted a joint fit of the spectra provided by EPIC and ISGRI data. This is justified by the fact that the source shows a low flux level in both ISGRI and EPIC data and that the ISGRI data fall on the extrapolation of the EPIC spectrum (the normalization of the ISGRI spectrum with respect to the EPIC spectrum is $C = 1.0 \pm 0.4$). We then argue that the blazar is in the same spectral state during the two observations, despite being separated by ~4 years. The joint fitting procedure found a single power-law function to be the best-fit model with parameters given in Table 2.

We performed a joint fit to the XRT observations and the BAT spectrum. Best-fit models are given in Table 2. We note that for the observation of 2005-12-13 the normalization of BAT with respect to XRT is higher than unity ($C = 2.3^{+2.2}_{-1.0}$): this probably reflects the flux variability of the source, given the fact that the BAT spectrum relates to data integrated over a period of 9 months. Since the XRT spectrum was retained as reference, we note that the model flux is comparable to that obtained for the EPIC+ISGRI spectrum.

3. Discussion

3.1. Spectral variation

The present analysis, and past results, shows that the hard-X-ray emission in the ~60−300 keV interval (object rest frame) of PKS 2149-306 does not vary in spectral shape: indeed spectra obtained almost a year apart by *INTEGRAL*/ISGRI and *Swift*/BAT show a constant (within errors) photon index, which is also consistent with the slope previously inferred for data acquired by *BeppoSAX* in 1997 ($\Gamma = 1.37 \pm 0.04$ – Elvis et al. 2000). We recall that the spectra refer to an average state covering ~10 days for ISGRI and ~9 months for BAT. Despite the lack of spectral variability, the integrated flux in the 20−100 keV band exhibits a variation of more than a factor of two from the lowest value of ISGRI to the highest value for BAT. A remarkable change in the hard-X-ray flux is not uncommon for blazars, and it was observed, for instance, in *Swift* J1656.3-3302, although with a different spectral slope (Masetti et al. 2007).

In the 0.2−10 keV energy band, our data analysis suggests a more complex behavior. As discussed in Ferrero & Brinkmann (2003), the source spectrum acquired in 2001
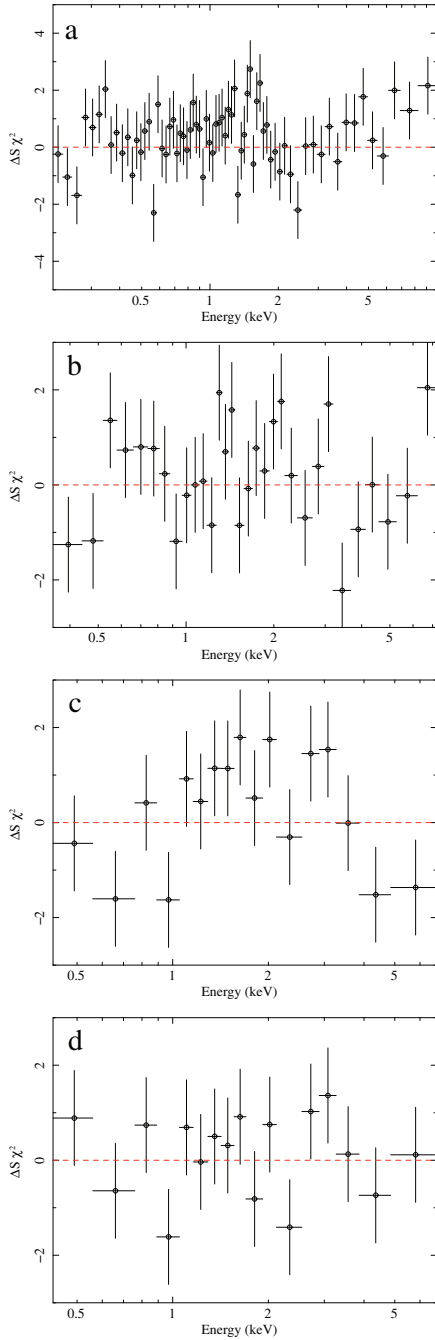
Fig. 1. Residual plots in units of σ with error bars of size 1 sigma. *panel* **a**): *XMM-Newton* data with respect to a power-law model in the object rest frame with Galactic absorption; *panel* **b**): XRT (2005-12-10) with a single power-law; *Panel* **c**): XRT (2005-12-13) with a single power-law; *panel* **d**): XRT (2005-12-13) using a broken power-law model.

(*XMM-Newton*/EPIC data) is well described by a single power-law function with little evidence that a more complex model is necessary. Instead, the two observations with XRT in 2005 suggest a spectral change from a power-law model in the first observation (2005-12-10), to a curved model in the second pointing (2005-12-13), with a hint of curvature developing over ~3 days. As for other high-z radio-loud quasars, this feature is usually interpreted as an extra-absorption component. This absorbing cloud should be associated with the quasar frame, since no Damped Lyα features reveal absorption by intervening material.
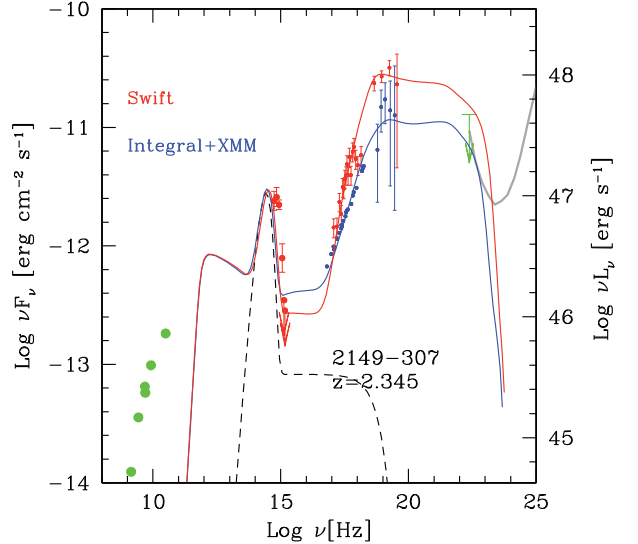

Fig. 2. Spectral Energy Distributions and models (solid lines) for *Swift* (red) and *XMM-Newton*+ISGRI (blue) data. The figure shows in green archival radio and IR data (from NED) and the EGRET upper limit (Fichtel et al. 1994). The gray line represents the *GLAST* sensitivity curve. The dashed line shows the input spectrum from the disk and the corona.

Although short-term variability due to changes in the intrinsic absorption was observed in Seyfert galaxies (Risaliti et al. 2007), a variation on time intervals of days is difficult to reconcile with the blazar picture since the absorbing cloud should be located at a distance of ~10^{15} cm from the black hole, below the length scale on which jet dissipation is supposed to occur in this class of objects. On the other hand, in the blazar scenario the soft photon deficit and its variation can be naturally interpreted as a spectral break due to the Inverse Compton regime onset (Tavecchio et al. 2007; Sambruna et al. 2007). Indeed a low-energy roll-off appears to be a common property of FSRQs, for distant objects such as MG3 J225155+2217 ($z = 3.668$, Maraschi et al. 2008), RBS 315 ($z = 2.69$, Tavecchio et al. 2007), and nearby FSRQs such as 3C 454.3 ($z = 0.859$, Ghisellini et al. 2007). For high-z FSRQs, the break signature falls in the soft X-ray band, where this feature can be blurred by contribution from the primary seed photon input and the bulk Comptonization of cold electrons in the jet (Celotti et al. 2007). Apart from spectral analysis, a variability study of simultaneous data in the optical to X-ray bands can provide clues to the origin of the intrinsic curvature in the continuum (Foschini 2008).

3.2. SED modeling

We define two different states of PKS 2149-306: a "low-flux" state given by *XMM-Newton* and *INTEGRAL* points and a "high-flux" state studied with XRT and BAT data, for which we obtained a high flux level separately in the [2−10] and [20−100] keV band. We chose the second observation of XRT (on 2005-12-13), since the flux is comparable to the first one but exhibits spectral bending at low energies. In Fig. 2 the SEDs for both states are depicted separately in blue and red. Optical/UV data were corrected for Galactic absorption according to Cardelli et al. (1989) and using the zero points given in the calibration files. X-ray points are corrected only for the Galactic absorption. The multiwavelength spectra are completed with radio and

Table 3. SED model parameters. See text for more details.

Parameter	*Swift*	EPIC+ISGRI
$R(10^{15}$ cm)	15	15
$h(10^{15}$ cm)	150	150
Θ(deg)	3	3
Γ_{bulk}	15	10
$L_{\text{inj}}(10^{43}$ erg s^{-1})	8	8
γ_{break}	5	5
γ_{max}	1000	1000
B(G)	3.3	3.3
$L_{\text{disk}}(10^{45}$ erg s^{-1})	150	150
$R_{\text{BLR}}(10^{15}$ cm)	1300	1300

IR data taken from NED, and the EGRET upper limit (Fichtel et al. 1994).

We attempt to describe the two states in terms of changes in the physical parameters of the source. For both, we model the source as discussed in detail in Ghisellini et al. (2002). The model assumes synchrotron and Inverse Compton emission from a spherical region in the jet, of radius R, at a distance h from the disk, with bulk Lorentz factor Γ and orientation Θ with respect to the line of sight. The blob is populated by a tangled and homogeneous magnetic field B and by relativistic electrons, injected with total power L_{inj} and a broken power-law energy distribution described by γ^{-1} in $[1, \gamma_{\text{break}}]$, and $\gamma^{-3.2}$ up to γ_{max}. The model accounts for radiative losses and determines the cooling energy γ_{cool} of particles after a dynamical time R/c (see e.g., Maraschi et al. 2008). The primary emission is provided by a disk and a tenuous corona with a power-law spectrum of slope $\alpha = 1$ and cut-off at 150 keV. The disk spectrum is described by a black-body peaking at $\nu_0 \sim 10^{15}$ Hz and with power L_{disk}, derived from the optical/UV spectral data. For the *XMM-Newton+INTEGRAL* state, we can place only weak constraints on the disk/corona emission, because of the lack of data from the optical monitors of both satellites. However, the upper limit of *XMM-Newton*/OM in the *UV* band and the almost constant archival optical data suggest that the soft photon input for the Inverse Compton regime does not vary significantly in the two states. The Broad Line Region (BLR), located at R_{BLR} from the central black hole (see e.g., Ghisellini & Madau 1996), reflects the primary emission toward the jet with luminosity $L_{\text{BLR}} = 0.1 L_{\text{disk}}$ (Kaspi et al. 2005).

We attempted to reproduce both states by varying as small a number of parameters as possible. This choice was also motivated by the limited energy range covered by the available simultaneous data. The absence of information above hundreds of keV makes the high energy electron distribution poorly determined. The synchrotron regime is also poorly constrained because of the lack of data. This is, however, unimportant for the SED modeling, since the radio-IR emission includes contributions from the outer regions of the jet and, therefore, is not considered in this model.

Input model parameters for both states are given in Table 3. The overall SED of PKS 2149-306 is typical of FSRQs at high redshift, with the Inverse Compton mechanism dominating the spectrum from X- to γ-rays and in accordance with the standard blazar sequence (Maraschi et al. 2008).

The two different SEDs can be explained in terms of a change only in the jet bulk Lorentz factor, being $\Gamma = 15$ for the "high-flux" state and $\Gamma = 10$ for the "low-flux" state. The different Lorentz factors of the emitting region can be interpreted in terms of the inner-shock model scenario (e.g., Spada et al. 2001),

which assumes that subsequent colliding shells at different speed produce a new radiating shell with intermediate Γ. The variation in the Γ Lorentz factor accounts for the change in the total power of the source and for the spectral changes in the Inverse Compton regime, observed in the SEDs for the two states. In the "low-flux state" (found in *XMM-Newton* and *INTEGRAL* data), the "low" Γ drives a "cooling branch" in the electron distribution with $\gamma_{\text{cool}} = 12$ and a slope 2.2 in $[\gamma_{\text{peak}}, \gamma_{\text{cool}}]$. This cooling branch does not develop in the "high-flux" state, since we found that $\gamma_{\text{cool}} \sim \gamma_{\text{break}}$.

The present data quality and the partial simultaneous spectral coverage limit a careful inspection of all full model input parameter range. However, it is remarkable that the two spectral states are described by changing only the jet bulk Lorentz factor; this parameter accounts for both the flux variation and the spectral change of the Inverse Compton spectra. More complex solutions, changing more than one parameter, are not excluded, although we propose the simplest and physically consistent explanation of the state variation for the source.

4. Conclusions

We have investigated the long-term behavior of the blazar PKS 2149-306 ($z = 2.345$). All *XMM-Newton*, *Swift*, and *INTEGRAL* publicly available data have been reprocessed and analyzed with the latest software versions and calibration data bases. The SED, compiled with the data analyzed in the present work complemented with those available in the archives, is typical of FSRQs at the brightest end of the blazar sequence.

Swift observations suggest a hint of a roll-off below ~1 keV emerging on ~3-day timescale, which can be explained as the natural spectral break due to the Inverse Compton onset. However, the present data quality does not allow us to distinguish firmly between the absorption/curvature dichotomy, and further multiband and simultaneous observations are necessary.

In the $60-300$ keV energy band (in the blazar frame), the flux levels derived from ISGRI and BAT data differ by more than a factor of two, without spectral slope variation. From the broadband spectral analysis, we can identify two different states: one found in data until 2004 (*XMM-Newton* and *INTEGRAL*), and another referring to a *Swift* observation performed in 2005. The SED modeling shows that the two states can be reproduced by changing only the bulk Lorentz factor of the jet.

References

Barthelmy, S. D., Barbier, L. M., Cummings, J. M., et al. 2005, Space Sci. Rev., 120, 143
Baumgartner, W., Tueller, J., Mushotzky, R., et al. 2008, ATel 1429
Bird, A. J., Malizia, A., Bazzano, A., et al. 2007, ApJS, 170, 175
Burrows, D. N., Hill, J. E., Nousek, J. A., et al. 2005, Space Sci. Rev., 120, 165
Cappi, M., Matsuoka, M., Comastri, A., et al. 1997, ApJ, 478, 492
Cardelli, J. A., Clayton, G. C., & Mathis, J. S. 1989, ApJ, 345, 245
Celotti, A., Ghisellini, G., & Fabian, A. C. 2007, MNRAS, 375, 417
Courvoisier, T. J. L., Walter, R., Beckmann, V., et al. 2003, A&A, 411, L53

Elvis, M., Fiore, F., Siemiginowska, A., et al. 2000, ApJ, 543, 545
Fang, T., Marshall, H. L., Bryan, G. L., & Canizares, C. R. 2001, ApJ, 555, 356
Ferrero, E., & Brinkmann, W. 2003, A&A, 402, 465
Fichtel, C. E., Bertsch, D. L., Chiang, J., et al. 1994, ApJSS, 94, 551
Foschini, L., Ghisellini, G., Raiteri, C. M., et al. 2006, A&A, 453, 829
Foschini, L. 2008, Adv. Space Res., accepted [arXiv:0807.2253v1]
Francis, P. J., Whiting, M. T., & Webster, R. L. 2000, PASA, 53, 56
Ghisellini, G., & Madau, P. 1996, MNRAS, 280, 67
Ghisellini, G., Celotti, A., & Costamante, L. 2002, A&A, 386, 842
Ghisellini, G., Foschini, L., Tavecchio, F., & Pian, E. 2007, MNRAS, 382, L82
Goldwurm, A., David, P., Foschini, L., et al. 2003, A&A, 411, L223
Kalberla, P. M. W., Burton, W. B., Hartmann, D., et al. 2005, A&A, 440, 775
Kaspi, S., Maoz, D., Netzer, H., et al. 2005, ApJ, 629, 61
Lebrun, F., Leray, J. P., Lavocat, P. et al. 2003, A&A, 411, L141
Maraschi, L., Foschini, L., Ghisellini, G., et al. 2008, MNRAS, 391, 1981
Masetti, N., Mason, E., Landi, R., et al. 2008, A&A, 480, 715
Mason, K. O., Breeveld, A., Much, R., et al. 2001, A&A, 365, L36
Ojha, R., Fey, A. L., Charlot, P., et al. 2005, AJ, 130, 2529

Page, K. L., O'Brien, P. T., Reeves, J. N., & Turner, M. J. L. 2004, MNRAS, 347, 316
Page, K. L., Reeves, J. N., O'Brien, P. T., & Turner, M. J. L. 2005, MNRAS, 364, 195
Risaliti, G., Elvis, M., & Fabbiano, G., et al. 2007, ApJ, 659, L111
Roming, P. W. A., Kennedy, T. E., Mason, K. O., et al. 2005, Space Sci. Rev., 120, 95
Sambruna, R. M., Tavecchio, F., Ghisellini, G., et al. 2007, ApJ, 669, 884
Siebert, J., Matsuoka, M., Brinkmann, W., et al. 1996, A&A, 307, 8
Spada, M., Ghisellini, G., Lazzati, D., & Celotti, A. 2001, MNRAS, 325, 1559
Strüder, L., Briel, U., Dennerl, K., et al. 2001, A&A, 365, L18
Tavecchio, F., Maraschi, L., Ghisellini, G., et al. 2007, ApJ, 665, 980
Tueller, J., Mushotzky, R. F., Barthelmy, S., et al. 2008, ApJ, 681, 113
Turner, M. J., Abbey, A., Arnaud, M., et al. 2001, A&A, 365, L27
Ubertini, P., Lebrun, F., Di Cocco, G., et al. 2003, A&A, 411, L131
Yaqoob, T., George, I. M., Nandra, K., et al. 1999, ApJ, 525, L9
Wilkes, B. J. 1986, MNRAS, 218, 331